Journal of Applied Physics ARTICLE pubs.aip.org/aip/jap

Effective hydrogen diffusivity in n- and p-type crystalline silicon from 300 to 450 °C

Cite as: J. Appl. Phys. **139**, 035702 (2026); doi: 10.1063/5.0300191
Submitted: 31 August 2025 · Accepted: 24 December 2025 ·
Published Online: 20 January 2026

Zhuofeng Li,[1,a)] Zhongshu Yang,[1] Jiali Wang,[1] AnYao Liu,[1] Areebah Murad,[1] Chang Sun,[2] Wei Han,[2] Yichun Wang,[2] Hieu Nguyen,[1] and Daniel Macdonald[1,a)]

AFFILIATIONS

[1]School of Engineering, Australian National University, Canberra, Australia
[2]R&D Center-Wafer B.U LONGi Green Energy Technology Co., Ltd., Shaanxi, China

[a)]**Authors to whom correspondence should be addressed:** zhuofeng.li@anu.edu.au and daniel.macdonald@anu.edu.au

ABSTRACT

We study hydrogen diffusion in silicon by annealing wafers with hydrogen-rich aluminum oxide layers on one surface and intrinsic PECVD silicon films acting as a hydrogen capture sink on the other surface. The hydrogen concentration in the silicon film is monitored via spectrally resolved sub-bandgap photoluminescence, calibrated by comparison with time-of-flight secondary ion mass spectrometry measurements. This provides a convenient and rapid method for hydrogen concentration measurements. Modeling the kinetics of the increasing hydrogen concentration in the silicon film as hydrogen diffuses through the wafer allows the effective hydrogen diffusivity to be extracted at annealing temperatures of 300–450 °C, a range that is relevant for silicon solar cell technology, but has not often been directly measured. The extracted hydrogen diffusivities in undoped silicon and both moderately and heavily doped n- and p-type silicon are compared with the existing literature reports. The results match very well with the model of Herring *et al.* for moderately doped n-type and undoped silicon. For heavily doped n-type and p-type silicon with different dopant concentrations, however, we report significantly reduced effective hydrogen diffusivity values. Finally, we present the modeling of hydrogen charge states in differently doped silicon and consider possible explanations for the reduction in effective hydrogen diffusivity.

I. INTRODUCTION

Hydrogen plays a crucial role in passivating surface and bulk defects in crystalline silicon (c-Si) solar cells.[1–10] During device fabrication, hydrogenation typically takes place during thermal annealing in the presence of hydrogen-rich films such as silicon nitride (SiN_x)[1–8] and aluminum oxide (Al_2O_3).[9,10] These films release hydrogen that passivates defects both at the interfaces and within the c-Si wafer bulk, thereby improving the electrical properties of the device.[7–9] One important determinant of the effectiveness of hydrogenation is the diffusivity of monatomic hydrogen in the c-Si substrate. This can depend on the hydrogen charge states and their interaction with charged dopants and defect states in the c-Si bulk.[8,9] Multiple studies using various experimental techniques have reported effective hydrogen diffusivity values in c-Si across a wide range of temperatures, often differing by orders of magnitude at a given temperature.[11–20] A significantly reduced diffusivity was reported in c-Si containing impurities, which could trap hydrogen.[14] Decreased hydrogen diffusivities were also reported in heavily doped n-type Si[20] and in p-type Si in which hydrogen can be temporarily trapped by charged dopant atoms.[17,19] Some reports suggested that the hydrogen charge states can directly alter the diffusion barrier height.[15,21–23] An improved understanding of these effects is important for optimizing the benefits of hydrogenation in Si solar cells.[11,24–28]

Generally, the temperature dependence of monoatomic hydrogen diffusion in c-Si is described via an Arrhenius equation for the effective hydrogen diffusivity D_H,

$$D_H = D_0 \exp\left(\frac{-E_a}{k_B T}\right), \tag{1}$$

where k_B and T represent the Boltzmann constant and absolute temperature, respectively, while E_a denotes the effective activation energy for diffusion, and D_0 is a constant pre-exponential factor.

The reported values of E_a are reasonably consistent, mostly falling in the range $E_a = 0.5 \pm 0.05$ eV. On the other hand, there is a much greater discrepancy in the pre-exponential factor D_0, which spans four orders of magnitude from 9.4×10^{-3},[12] to 9×10^{-7} cm^2 s^{-1},[14] which, in turn, leads to large discrepancies in the reported D_H values. This is consistent with the impact of temporary trapping at defects and charged dopants, which effectively reduces the average attempt frequency for hydrogen diffusion and, in turn, reduces the value of the pre-exponential factor D_0.

In this work, we demonstrate a method that allows the effective diffusivity of hydrogen in c-Si to be determined at temperatures between 300 and 450 °C, a temperature range that is less often reported in the literature and difficult to form stable trapping sites.[11] Hydrogen-rich Al_2O_3 layers are deposited on one surface of a c-Si wafer, which releases hydrogen during annealing. A hydrogen sink on the other surface of the wafer captures the released hydrogen atoms as they diffuse through the c-Si substrate, as shown in Fig. 1. In this work, we use PECVD (plasma enhanced chemical vapor deposition) deposited Si films as the hydrogen sink, which were initially de-hydrogenated through annealing before depositing the hydrogenated Al_2O_3 layer on the other side. These PECVD deposited Si films are widely used in c-Si solar cell technology, such as the intrinsic amorphous Si interlayers in heterojunction devices.[29,30] Such films are usually hydrogenated when deposited but can be effectively de-hydrogenated upon annealing, as will be shown later in this paper. The hydrogen content can be measured by secondary ion mass spectrometry (SIMS) for the hydrogen isotope deuterium[31,32] and time-of-flight SIMS (ToF-SIMS) for monatomic hydrogen.[33,34]

Here, we use ToF-SIMS to measure the hydrogen concentrations in the deposited Si films. However, these measurements are time-consuming. We, therefore, use ToF-SIMS measurements to calibrate an alternative, more rapid method for detecting hydrogen in the Si films, based on steady-state spectrally resolved photoluminescence (PL) measurements. A broad peak in the sub-bandgap PL spectrum has been reported for the hydrogenated, deposited Si films, with the peak intensity increasing with the amount of hydrogen present.[35–37] Here, we establish a direct empirical correlation between the sub-bandgap PL intensity and the ToF-SIMS-measured hydrogen concentration, enabling PL measurements to provide a rapid relative measurement of the hydrogen concentration in the deposited Si films.

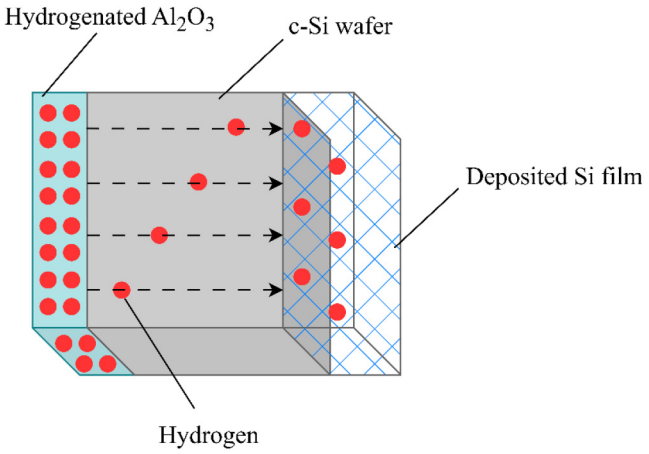

FIG. 1. Schematic of hydrogen migration in the test structure used in this work. Annealing releases hydrogen atoms from the Al_2O_3 layer. After diffusing through the c-Si wafer bulk, hydrogen is then captured by the defects in the deposited Si film on the opposite surface.

When applied to the samples subject to annealing for different durations at a given temperature, the effective hydrogen diffusivity can be extracted by fitting the hydrogen concentration kinetics in the deposited Si films. An implicit finite difference method is adapted to model the transport of hydrogen, accounting for the release of hydrogen from the source layers, diffusion through the wafer bulk, and capture at the sink films, similar to well-known impurity gettering processes,[38,39] as described in Sec. IV. This allows the effective hydrogen diffusivity in the c-Si wafer bulk to be determined at a given annealing temperature. The charge state modeling shows that in moderately doped n-type Si, hydrogen is mostly positively charged (H^+), while in heavily doped n-type Si with a dopant density $N_D > 1 \times 10^{18}$ cm^{-3}, it is mostly negatively charged (H^-).[40] In contrast, H^+ is dominant in both moderately and heavily doped p-type Si. By combining recent knowledge of different charge states of hydrogen in c–Si,[11,25–28,40] we discuss possible explanations for the observed changes in the effective hydrogen diffusivity.

II. EXPERIMENTAL WORK

In this work, we used Czochralski (Cz) grown c-Si wafers with varying dopant species, concentrations, and wafer thicknesses, as listed in Table I. Most of the wafers were provided by LONGi Green Energy. For the moderately doped Si wafers on the order of 10^{15}–10^{16} cm^{-3}, dark conductance measurements were used to determine the resistivity. For the heavily doped Si wafers on the order of 10^{18} cm^{-3}, electrochemical capacitance–voltage (ECV) profiling was employed to measure the dopant densities. The resistivity value of 12 000 Ω cm reported for the undoped Si wafer was cited from LONGi Green Energy, although the exact value was uncertain due to residual dopants. We estimate the dopant density of the undoped sample to be less than 1×10^{12} cm^{-3}. All wafers were etched in a tetramethyl ammonium hydroxide (TMAH) solution, were then subject to a standard RCA (Radio Corporation of America) cleaning process, and were then deposited with ∼50 nm thick intrinsic amorphous Si films on one side. The deposition was carried out in a Roth and Rau AK400 PECVD reactor for 3 min, at a set temperature of 500 °C, and a substrate temperature between 250 and 300 °C.[41,42] The thickness of the deposited amorphous Si layers was confirmed by spectroscopic ellipsometry.

Initially, after the PECVD amorphous Si deposition on one side of the wafer surface, a set of 150 μm thick moderately phosphorus-doped Si samples with $N_D = 2.6 \times 10^{15}$ cm^{-3} were annealed in a quartz tube furnace in N_2 at 550 and 600 °C for varying durations. This caused different extents of de-hydrogenation of the PECVD deposited Si films, as measured by spectral PL and ToF-SIMS, resulting in a representative range of

TABLE I. Resistivity, dopant densities, and thicknesses of the c-Si wafers.

Intentional doping	Resistivity (Ω cm)	Dopant density $N_{D/A}$ (cm^{-3})	Thickness W (μm)
Phosphorus	1.8	2.6×10^{15}	75, 150, and 350
	0.02	1.2×10^{18}	75
Antimony	0.7	6.3×10^{15}	120
Undoped	12 000 (estimated)	$<1 \times 10^{12}$	120
Boron	2.5	5.7×10^{15}	75 and 150
	0.02	4.2×10^{18}	75
Gallium	0.7	2.3×10^{16}	75

hydrogen concentrations remaining in the films. These samples were prepared for hydrogen concentration measurements by ToF-SIMS, allowing calibration of the sub-bandgap PL intensity as a proxy measurement of the hydrogen concentration.

Subsequently, after a standard RCA cleaning process, the remaining samples underwent thermal annealing in a quartz tube furnace at 600 °C in N_2 for 30 min, which will be shown in Sec. III, to effuse a significant amount of hydrogen out of the PECVD deposited Si films, resulting in hydrogen-lean Si films.[43] While as-deposited, the PECVD Si film was predominantly amorphous, the annealing step could induce partial crystallisation.[44] Therefore, to accurately reflect its post-anneal microstructure, which was neither purely amorphous nor fully polycrystalline, we refer to it as a deposited Si film in this study. After this de-hydrogenation step, all samples were then deposited with 25 nm thick hydrogenated Al_2O_3 films using FlexAL plasma assisted atomic layer deposition (PAALD) on the opposite side of the structure,[9,10] as shown by the schematic in Fig. 1. The deposition process took 25 min and was carried out at 200 °C, with negligible wrap-around effects.

With the sample structure shown in Fig. 1, annealing was then performed for different durations at 300, 350, 400, and 450 °C in a temperature-controlled THMS600 Linkam stage, releasing hydrogen from the Al_2O_3 films, which then diffused through the c-Si wafer bulk, and subsequently reached the deposited Si films on the other sides of the samples. We will later verify this in Sec. V A by measuring the effective hydrogen diffusivity in n-type samples with different wafer thicknesses. Given that the cm-sized samples were uniform, they were cleaved into smaller pieces and a new piece was used for each annealing duration, rather than conducting a cumulative annealing process on a single sample.

The annealing step activated the diffusion of hydrogen through the sample, although effusion could occur simultaneously, whereby hydrogen escaped from the Al_2O_3 passivating layer into the ambient. If hydrogen from the ambient were captured by the deposited Si film, it could lead to unexpected hydrogenation and distort the diffusivity measurement results. A control experiment was, therefore, conducted at 450 °C by annealing two different sample structures side by side. We used the 150 μm thick phosphorus-doped Si wafer with $N_D = 2.6 \times 10^{15}$ cm^{-3} and deposited one side with the de-hydrogenated Si film. For the opposite side, one sample was deposited with the Al_2O_3 passivating layer, while the other sample was not deposited with Al_2O_3. This experiment showed that hydrogen effusion into the ambient had no significant impact on the hydrogenation in the deposited Si films on the rear sides of the samples, as will be demonstrated in Sec. V A. Therefore, we are able to conclude that hydrogen accumulation in the deposited Si films occurred predominantly due to hydrogen diffusion through the c-Si bulk.

The PL spectra of the Si films on the rear side of the samples were measured at 80 K using a confocal Horiba iHR 320 mm spectral PL tool, equipped with a liquid N_2 cooled InGaAs detector.[36,37,42,45] An excitation wavelength of 405 nm was employed to illuminate the samples through a 50× objective lens, which is strongly absorbed by the thin deposited Si layers near the surface.[42,45] The on-sample power was 120 μW, with an illumination spot size of ~5 μm in diameter. The cooling to 80 K was accomplished by liquid N_2 in a Linkam stage. The PL signal emitted from the deposited Si films was captured within a $10 \times 10\,\mu m^2$ region, with nine measurements conducted on each sample to ensure repeatability and calculate the average PL spectra.

Example PL spectra from 900 to 1500 nm are shown in Fig. 2, measured on three samples subject to different degrees of de-hydrogenation. The PL signal from the Si film after de-hydrogenation at 600 °C shows negligible sub-bandgap

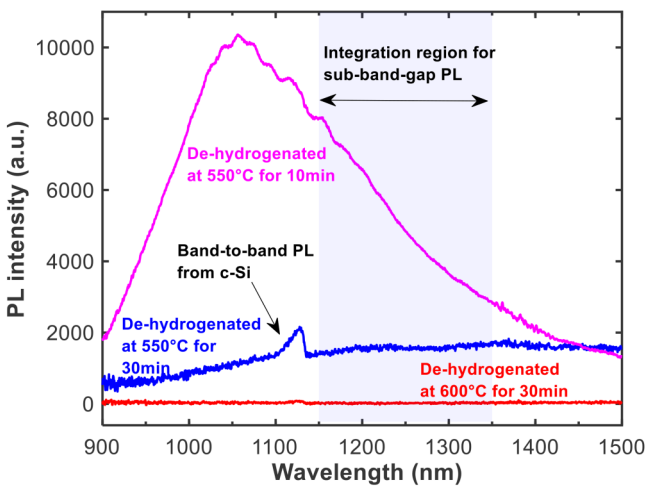

FIG. 2. PL spectra measured in samples subject to de-hydrogenation under different annealing conditions. The shaded region highlights the wavelength range between 1150 and 1350 nm used for the determination of the hydrogen concentration.

emission. For the sample annealed at 550 °C for 30 min, a significant concentration of hydrogen atoms remains in the Si film, and hence, the PL intensity is higher, with a sharp band-to-band peak at ~1130 nm from the c-Si substrate.[37] For the sample de-hydrogenated at 550 °C for 10 min, the sub-bandgap PL intensities are much stronger, due to higher concentrations of hydrogen in the film.[42] However, in this case, the band-to-band c-Si peak is masked by the sub-bandgap signal, forming a broad PL spectrum over a wide wavelength range. To avoid the band-to-band peak, the PL measurements were integrated between 1150 and 1350 nm as a representative measurement of the hydrogen concentration. The first set of samples were also subject to ToF-SIMS measurements to establish a calibration curve. The ToF-SIMS measurements were performed at the University of New South Wales in a negative polarity using a 30 kV Bi^+ primary ion beam for analysis, with 1 keV Cs^+ sputtering for depth profiling.

III. EMPIRICAL CALIBRATION OF PL INTENSITIES AND HYDROGEN CONCENTRATIONS

As shown in Fig. 3(a), the PL intensities emitted across the wavelength range between 1150 and 1350 nm decrease with increasing annealing time at a fixed temperature of 550 °C and reach a minimum after annealing at 600 °C for 30 min.[42,43] The hydrogen concentrations of these samples were also measured by ToF-SIMS from the surface to a depth of 90 nm, extending beyond the thickness of the Si films of around 50–60 nm, as shown in Fig. 3(b). Note that the as-measured SIMS intensity does not indicate absolute hydrogen concentrations due to the lack of a calibration standard. Nevertheless, the relative change in hydrogen concentrations with respect to the sample de-hydrogenated at 600 °C for 30 min is sufficient to determine a relative calibration curve.

Figure 3(c) shows the hydrogen concentrations integrated over a thickness of 60 nm from the ToF-SIMS measurements, as a function of integrated sub-bandgap PL intensities over the range from 1150 to 1350 nm. The sharp peaks of the SIMS signals close to the surface, as shown in Fig. 3(b), are excluded in the integration due to surface contamination and measurement artifacts. An empirical logarithmic fit is subsequently used to convert the measured PL intensities into relative hydrogen concentrations, as shown in Fig. 3(c).

IV. HYDROGEN DIFFUSION MODELLING

The diffusion analysis extracts the effective hydrogen diffusivity using a simplified Fickian diffusion model. The effective diffusivity is interpreted as a system-level transport coefficient that quantifies the net rate at which hydrogen moves from the Al_2O_3 source to the Si sink film under the specific experimental conditions in this study. By design, this parameter incorporates the cumulative influences of all processes present such as metastable interactions, which is suitable for comparative analysis between different c-Si samples. The model is, therefore, not intended to resolve microscopic diffusion kinetics including trap densities, binding energies, and reaction rates. Instead, it provides a robust macroscopic measure of hydrogen diffusion.

We employed an implicit finite difference method to numerically simulate the hydrogen diffusion process from the hydrogen-rich Al_2O_3 layer to the deposited Si film. The algorithm follows the unconditionally stable, implicit framework established for numerical iron gettering simulations by Hieslmair *et al.*[38] and Liu *et al.*[39] This approach was built upon the Crank–Nicolson method[46] but was developed to handle the specific equations of a diffusion-gettering model. According to the Dirichlet condition, we assumed the hydrogenated Al_2O_3 layer acted as an infinite source of hydrogen with a fixed hydrogen concentration value determined by the measured equilibrium hydrogen concentration, and the previously de-hydrogenated Si layer acted as an infinite hydrogen sink with a fixed value determined by the initial hydrogen concentration as measured in each dataset. These two boundaries are also discussed in Sec. V A. Further details can be found in the supplementary material. The effective hydrogen diffusivity in the c-Si wafer bulk is the only fitting parameter in the model and is used to match the measured hydrogen concentration kinetics to extract the effective hydrogen diffusivity in the c-Si wafer bulk.

V. RESULTS AND DISCUSSION

A. Verification of the method

To verify the hydrogen diffusivity measurement method proposed in this work, we first compare the extracted diffusivity results from two samples of the same doping but different wafer thicknesses, for which the extracted hydrogen diffusivity values are expected to be the same. Figure 4(a) shows the results of the phosphorus-doped Si wafer with $N_D = 2.6 \times 10^{15}\ cm^{-3}$ and with a wafer thickness of 150 μm, and Fig. 4(b) presents the wafer with the same dopant density but a different wafer thickness of 350 μm. In each case, the c-Si wafer bulk is much thicker than the deposited Si film, accounting for the steady transition period during the initial annealing process, in which hydrogen diffuses in the wafer bulk before reaching the deposited Si film. After this steady transition period, the defect states in the deposited Si film start to capture hydrogen. Consequently, the hydrogen concentration increases significantly for a certain period and then saturates at a level at which the hydrogen concentration is thought to reach a steady-state balance between hydrogen capture and release from the Si film. This equilibrium hydrogen concentration is used as a fixed value for the boundary condition at the Al_2O_3 surface, while the initial minimum hydrogen concentration in each dataset is used to find the other boundary condition at the Si film surface. Three simulated diffusion curves with different hydrogen diffusivities are displayed to span the measured time-dependent hydrogen concentration data, yielding a best fit, and upper and lower limits for the extracted hydrogen diffusivity values. These upper and lower fits are used to estimate uncertainty in the extracted diffusivity values. The same effective diffusivity values are utilized in Figs. 4(a) and 4(b) to fit the change in hydrogen concentrations, giving confidence in the extracted diffusivity values for the two wafer thicknesses.

To examine the impact of hydrogen effusion on hydrogenation in the deposited Si films, we annealed two 150 μm thick n-type samples side by side at 450 °C: one with the Al_2O_3 layer and one without (the control). The control sample data in Fig. 4(a) show a negligible impact, confirming minimal ambient hydrogenation interference. We, therefore, conclude that the hydrogenation of the Si films originates only from hydrogen diffusing through the c-Si bulk.

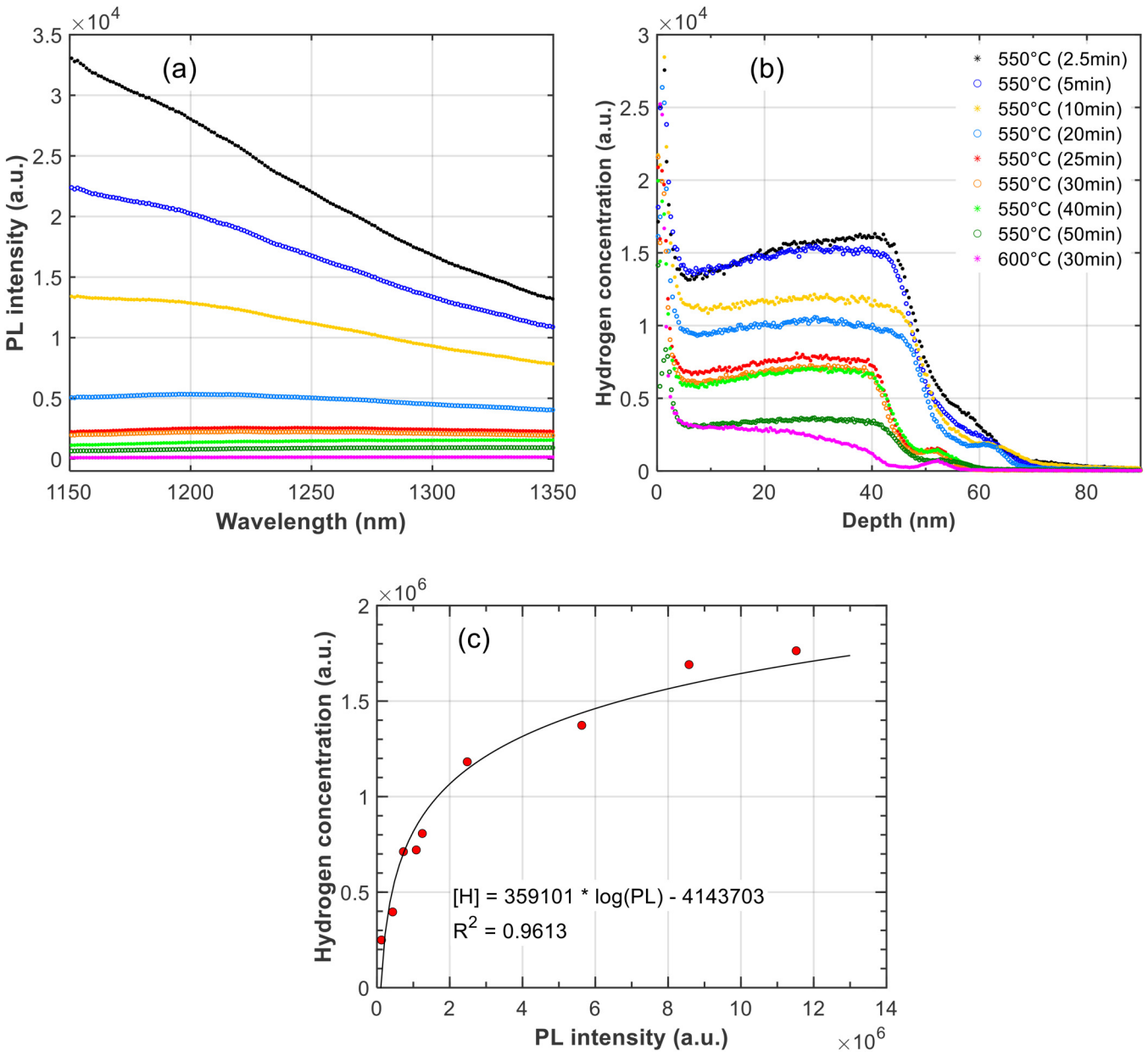

FIG. 3. (a) Sub-bandgap PL intensities emitted by the deposited Si films that were subjected to different annealing conditions. (b) Hydrogen concentration profiles for the same samples, as measured by ToF-SIMS. Graphs (a) and (b) share the same legend. (c) An empirical fit to convert the integrated PL intensity into relative hydrogen concentration.

B. Hydrogen diffusivity in n-type Si

Figure 5(a) presents the data obtained by annealing the 150 μm thick n-type Si samples with $N_D = 2.6 \times 10^{15}$ cm^{-3} at 350 and 400 °C, with only the best fit now shown in each case. The measurement at 300 °C shown in Fig. 5(b) was accomplished by utilizing a very thin wafer of 75 μm. By comparing Figs. 4, 5(a), and 5(b), the effective hydrogen diffusivity in the same phosphorus-doped Si is shown to reduce with decreasing temperature, as expected. The results for the undoped Si and antimony-doped Si at 400 °C are presented in Fig. 5(c) and are consistent with the effective diffusivity measured in the phosphorus-doped Si with $N_D = 2.6 \times 10^{15}$ cm^{-3}. Interestingly, the effective diffusivity is reduced in the

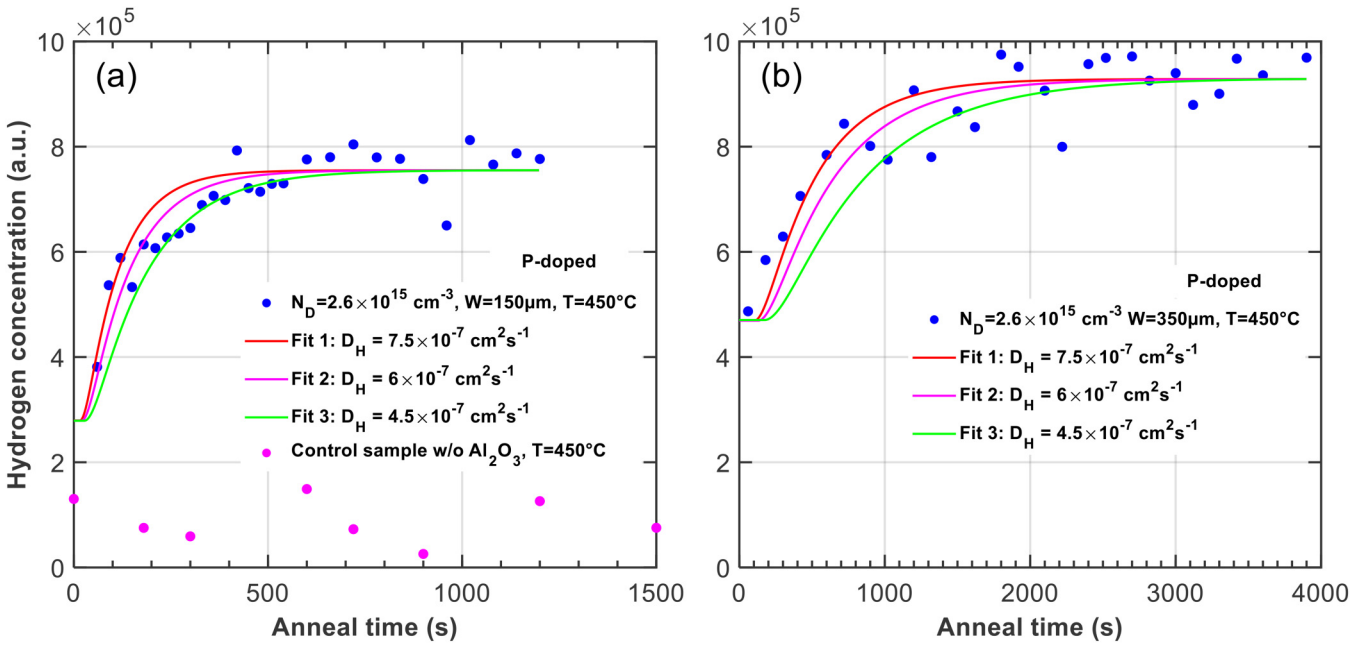

FIG. 4. Phosphorus-doped Si with $N_D = 2.6 \times 10^{15}$ cm^{-3} annealed at 450 °C under two conditions. (a) Wafer thickness of 150 μm, with three fits indicating the range of diffusivity values that span the variations in the measured data. The control sample without an Al_2O_3 film is also shown. (b) Wafer thickness of 350 μm with three fits using the same fitted diffusivity values as in (a).

heavily phosphorus-doped Si with $N_D = 1.2 \times 10^{18}$ cm^{-3}, as shown in Fig. 5(d).

C. Hydrogen diffusivity in p-type Si

This work also reports effective hydrogen diffusivity results in p-type Si samples. Figure 6(a) plots the time-dependent hydrogen concentrations in boron-doped Si with dopant densities $N_A = 5.7 \times 10^{15}$ and 4.2×10^{18} cm^{-3}, along with their simulated diffusion curves. Similar to Figs. 5(a) and 5(b), a thicker moderately boron-doped wafer significantly increases the annealing time required to reach the steady state. Again, a consistent effective diffusivity value despite different wafer thicknesses implies a reliable estimation of the hydrogen diffusivity in p-type Si. In comparison, the annealing duration for the 75 μm thick heavily boron-doped Si sample is much longer than the moderately doped sample with the same thickness, resulting in a significantly reduced hydrogen diffusivity. The moderately boron-doped samples with a thickness of 75 μm were also annealed at 400 and 350 °C, with the effective diffusivity results shown in Figs. 6(b) and 6(c). Additionally, a gallium-doped wafer with $N_A = 2.3 \times 10^{16}$ cm^{-3} was measured and the result is presented in Fig. 6(d), showing diffusivity similar to that obtained in the moderately boron-doped wafer in Fig. 6(a).

D. Hydrogen diffusivity compared to literature

Figure 7 plots the effective hydrogen diffusivity values measured in this work in comparison with some published data. Among these results, the Arrhenius fit for hydrogen diffusion in c-Si was first established by van Wieringen and Warmholtz in 1956,[12] which extracted the diffusivity from hydrogen permeation through an ingot at high temperatures between 1092 and 1200 °C. At such high temperatures, hydrogen becomes ionized, and the dominant charge state shifts toward H^+ due to increased thermal energy and intrinsic carrier generation in the c-Si bulk.[11] Gorelkinskii and Nevinnyi identified H^+ diffusion in their experiment conducted at lower temperatures between 126 and 143 K,[18] whose work was summarized by Herring *et al.* to extrapolate the hydrogen diffusivity to a higher temperature range.[11] Herring *et al.* proposed a H^+ diffusivity model by performing time-resolved capacitance-transient measurements on phosphorus-doped Si with a dopant density $N_D \sim 1 \times 10^{16}$ cm^{-3}.[11] In this work, we present four data points measured in similarly moderately phosphorus-doped Si at elevated temperatures, which are shown to agree very well with the Arrhenius plot of Herring *et al.* The effective diffusivity values measured in the antimony-doped and undoped Si wafers at 400 °C also align with this Arrhenius plot in Fig. 7.

Notably, the heavily doped n-type Si and all of the p-type Si samples examined in this work show reduced hydrogen diffusivities as compared to the moderately doped n-type Si. Similar reductions have also been reported in p-type Si,[13,15,17,19] in defect-rich n-type[14] or heavily doped n-type Si.[20] Ichimiya and Furuichi published their model in 1968 by measuring the diffusivity from the out-diffusion of tritium in boron-doped Si with a high resistivity of 150 Ω cm,[13] at temperatures from 400 to 500 °C, similar to the temperature range in this work. As highly pure p-type Si might not induce strong hydrogen trapping in the wafer bulk, a possible

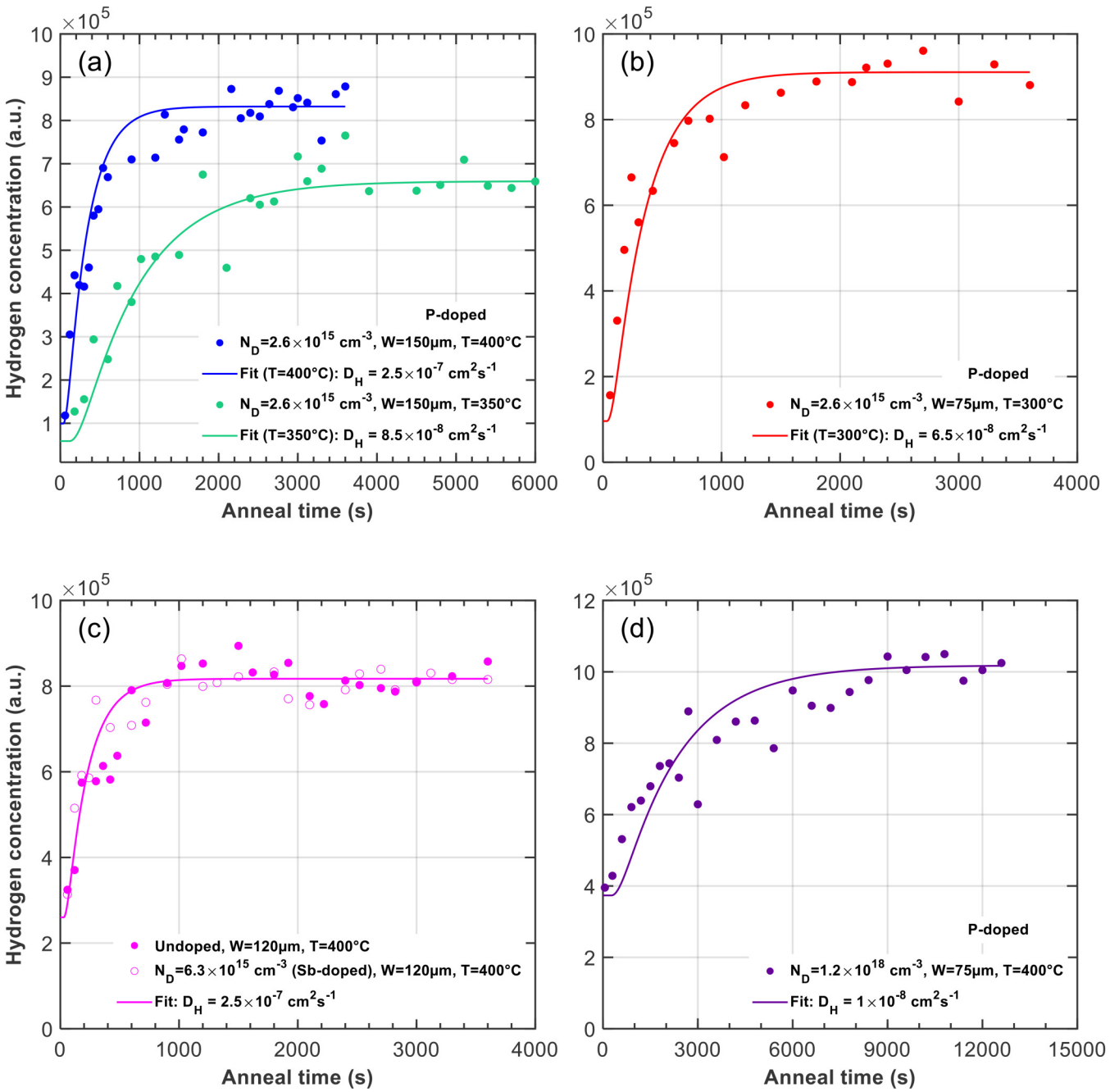

FIG. 5. (a) Phosphorus-doped ($N_D = 2.6 \times 10^{15}$ cm^{-3}) Si wafer with a thickness of 150 μm, annealed at 400 and 350 °C. (b) The same phosphorus-doped Si wafer in (a) but with a thickness of 75 μm and annealed at 300 °C. (c) Undoped and antimony-doped ($N_D = 6.3 \times 10^{15}$ cm^{-3}) Si wafers with a thickness of 120 μm and annealed at 400 °C. (d) Heavily phosphorus-doped ($N_D = 1.2 \times 10^{18}$ cm^{-3}) Si wafer with a thickness of 75 μm, annealed at 400 °C.

reason for such a low diffusivity value was speculated to be the incorporation of thin oxide layers that could block hydrogen transport.[13] Capizzi and Mittiga attributed the decrease in hydrogen diffusivity to a high effective energy barrier of $E_a = 0.8$ eV by measuring heavily doped p-type Si samples with N_A on the order of 10^{19} cm^{-3}.[15] The other literature reports suggested the reduction was due to hydrogen trapping by dopants or defects,[14,17,19,20] as discussed in Sec. V E based on hydrogen charge state modeling.

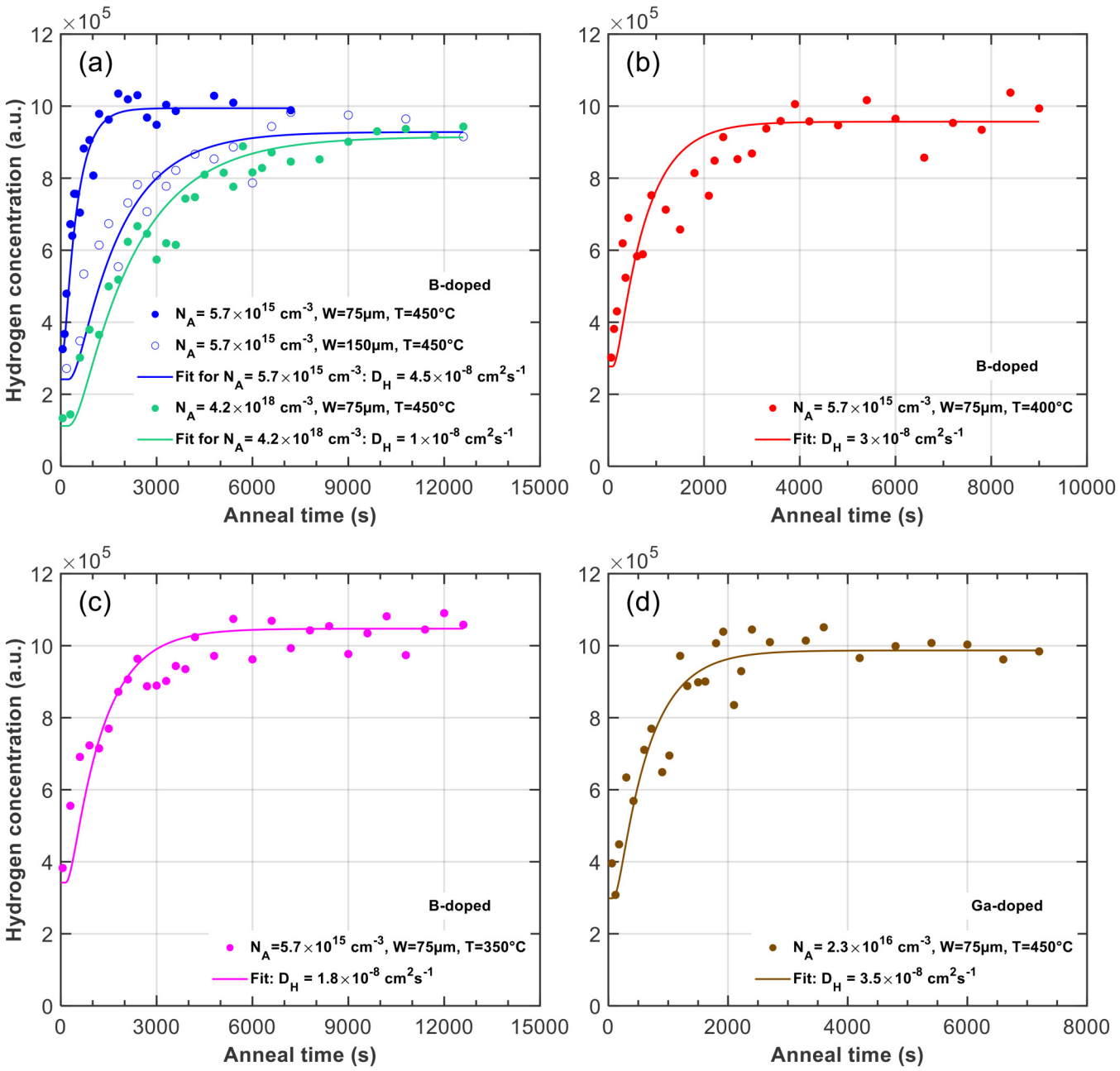

FIG. 6. Diffusivity results in p-type Si wafers. (a) Moderately boron-doped ($N_A = 5.7 \times 10^{15}$ cm^{-3}) Si with two thicknesses of 75 and 150 μm, and fitting curves applying the same diffusivity value in the modeling. Heavily boron-doped ($N_A = 4.2 \times 10^{18}$ cm^{-3}) Si with a thickness of 75 μm. All samples were annealed at 450 °C. (b) Moderately boron-doped ($N_A = 5.7 \times 10^{15}$ cm^{-3}) Si with a thickness of 75 μm, annealed at 400 °C. (c) Moderately boron-doped ($N_A = 5.7 \times 10^{15}$ cm^{-3}) Si with a thickness of 75 μm, annealed at 350 °C. (d) Gallium-doped ($N_A = 2.3 \times 10^{16}$ cm^{-3}) Si with a thickness of 75 μm, annealed at 450 °C.

For the moderately doped p-type Si with $N_A = 5.7 \times 10^{15}$ cm^{-3} measured in this study, effective diffusivity values are presented at temperatures between 350 and 450 °C. These experimental data are fitted with an Arrhenius plot in Fig. 7(b), which shows a fit by assuming $E_a = 0.5$ eV, similar to $E_a = 0.497$ eV given by Herring *et al.* and $E_a = 0.48$ eV by van Wieringen and Warmholtz.[11,12] This Arrhenius plot yields a D_0 value one order of magnitude lower than the fit by Herring *et al.*

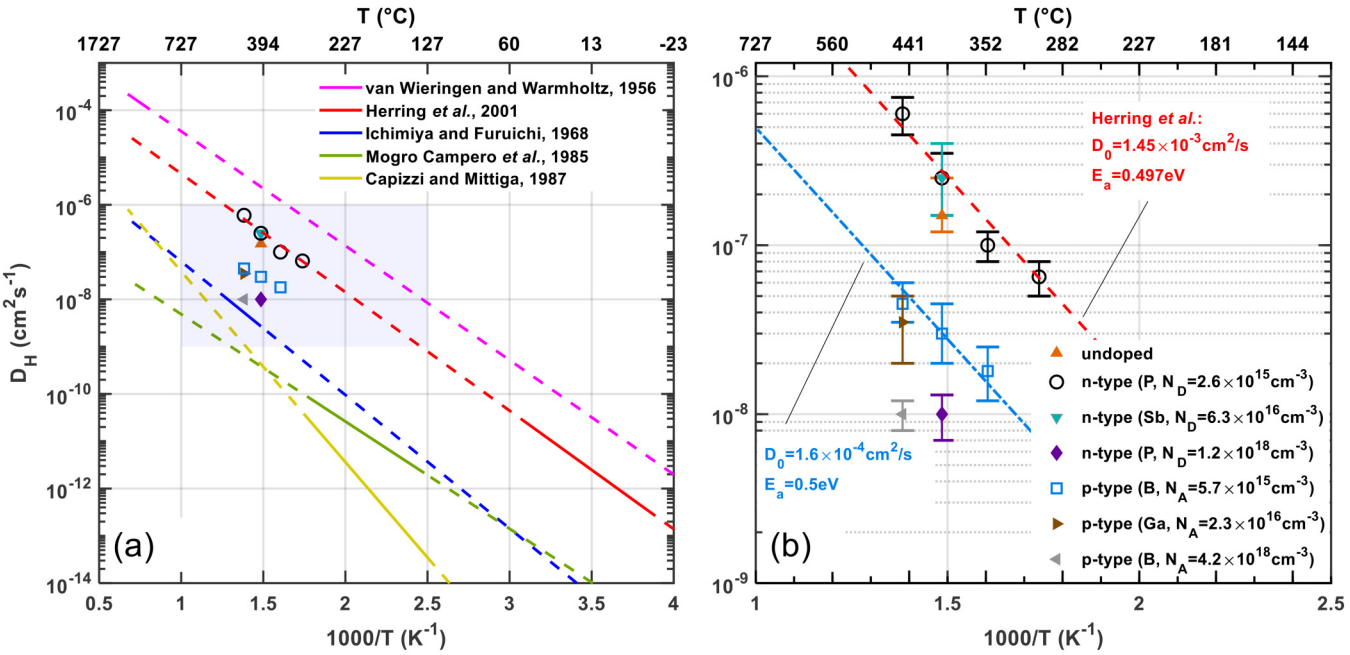

FIG. 7. Hydrogen diffusivities obtained in this work compared to published data and fits. (a) and (b) share the same legend, with (b) as a zoom-in graph for the shaded region in (a). The solid lines represent the actual temperature ranges used in other studies, whereas the dotted lines are extrapolated from the corresponding reported Arrhenius equations. The symbols in (a) are diffusivity values measured in this work, which are displayed with error bars in (b). The additional Arrhenius fit in (b) for the p-type Si ($N_A = 5.7 \times 10^{15}$ cm^{-3}) is plotted by assuming an activation energy of $E_a = 0.5$ eV.

E. Impact of hydrogen charge states on hydrogen diffusivity

We modeled the hydrogen charge states as a function of temperature for the dopant concentrations and types used in this work, according to Refs. 11, 40, and 47. Here, we assumed a donor level located 0.16 eV below the conduction band and an acceptor level positioned 0.064 eV below midgap.[11] Figure 8 shows the simulated fractional concentrations of the three monatomic hydrogen charge species H^+, H^0, and H^- in thermal equilibrium as a function of temperature. The shaded regions highlight the annealing temperature range applied in this work between 300 and 450 °C. In Fig. 8(a), which shows the moderately doped n-type Si case, the dominant charge state shows a transition from H^- to H^+ as the annealing temperature increases above 500 K. It is clear from Figs. 8(a) and 8(b) that within the applied annealing temperature range, the dominant charge state is H^+ in the moderately doped n-type Si, as opposed to predominantly H^- in the heavily doped n-type Si. The change in the dominant hydrogen charge state may decrease the effective hydrogen diffusivity. Similarly, Rizk *et al.* reported a much lower H^- diffusivity value of 1×10^{-13} cm^2 s^{-1} in a heavily phosphorus-doped sample with $N_D = 6 \times 10^{18}$ cm^{-3} at 120 °C, as compared to wafers with N_D on the order of 10^{16}–10^{17} cm^{-3} that showed a H^- diffusivity value of 7.5×10^{-13} cm^2 s^{-1}.[20] Mogro-Campero *et al.* introduced defect states by intentional gold doping in the n-type Si bulk, showing an Arrhenius plot with significantly decreased hydrogen diffusivity in Fig. 7(a).[14] They extracted an activation energy of $E_a = 0.45$ eV, similar to Refs. 11 and 12. However, Mogro-Campero *et al.* reported a very low $D_0 = 9 \times 10^{-7}$ cm^2 s^{-1}, which implies the defects acted as trapping centers and slowed hydrogen diffusion.

In Figs. 8(c) and 8(d), simulations show that H^+ consistently occurs as the majority charge state regardless of the p-type dopant density or temperature, which may explain the reduction in the measured diffusivity results compared to the values measured in the moderately doped n-type Si in Fig. 7. Zundel and Weber measured two moderately boron-doped Si wafers with dopant densities $N_A = 1.4 \times 10^{15}$ and 3.8×10^{16} cm^{-3}, which suggested non-linearity in the Arrhenius plot for hydrogen diffusivity values in p-type Si.[19] They summarized this non-linear behavior by introducing N_A into the Arrhenius equation. However, their equation does not fit with diffusivity results in the heavily doped p-type Si with N_A on the order of 10^{18}–10^{19} cm^{-3} as presented in this work or other literature studies.[15,17] Herrero *et al.* also suggested that trapping of hydrogen by acceptors is likely to occur in the heavily boron-doped Si bulk.[17]

F. Discussion

While several earlier studies attributed the reduction in effective hydrogen diffusivity to trapping by dopants[15,17,19,20] or defects,[14] these trapping effects were generally observed under low- and intermediate-temperature conditions. However, the reduction in the effective hydrogen diffusivity observed in our measurements

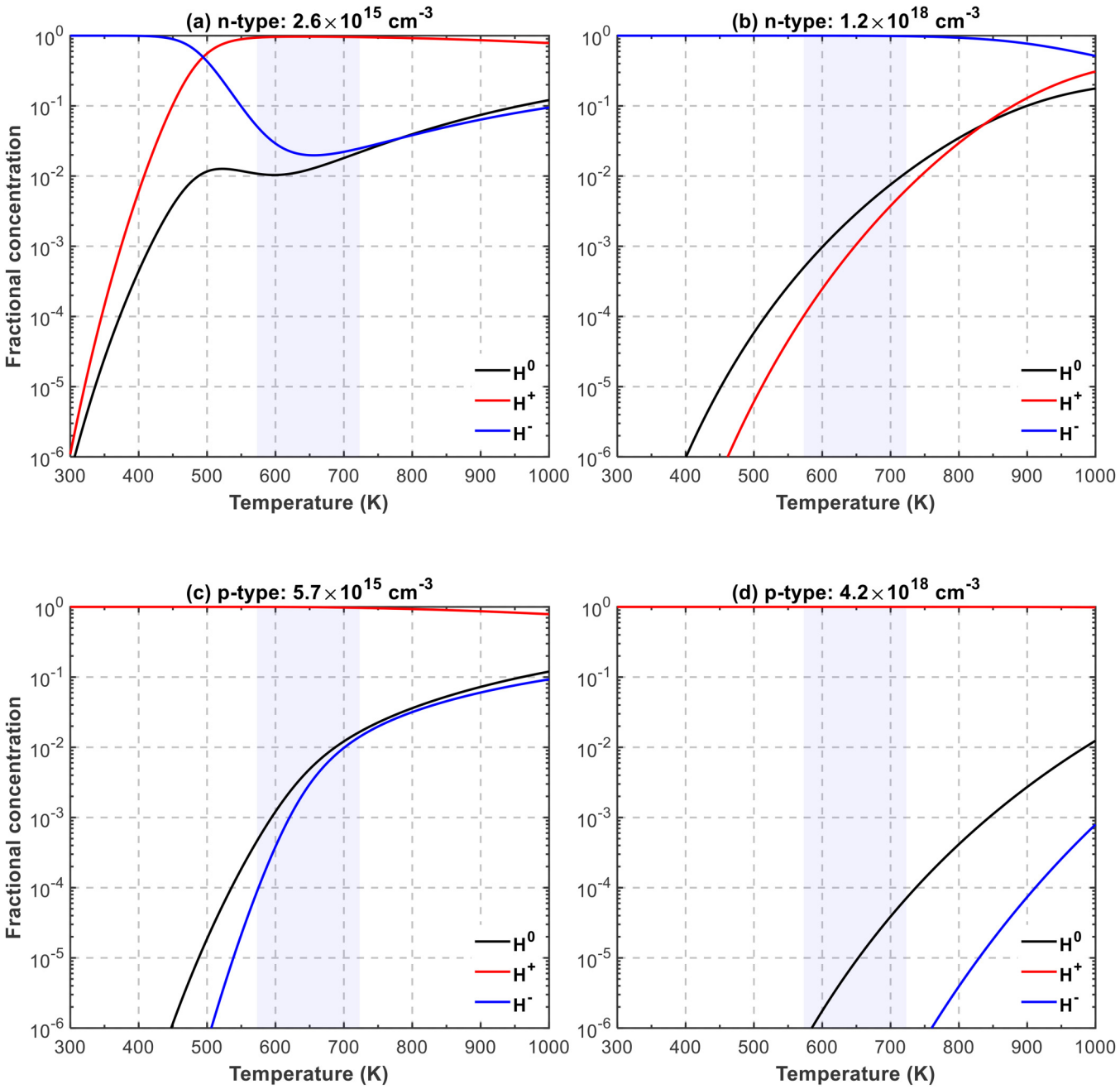

FIG. 8. Simulated fractional concentrations of different charge states of monatomic hydrogen in c-Si in thermal equilibrium. The shaded regions represent the temperature range between 300 and 450 °C as used in this work. (a) and (b) Moderately and heavily doped n-type Si. (c) and (d) Moderately and heavily doped p-type Si.

may not be attributed to the formation of stable dopant–hydrogen complexes. As demonstrated in Ref. 11, both phosphorus–hydrogen and boron–hydrogen complexes dissociate rapidly above 300 °C and, therefore, cannot persist at the temperatures used in this study. Instead, we propose that the doping-dependent reduction in hydrogen diffusivity arises from the cumulative, transient impact of metastable hydrogen configurations on the high-temperature diffusion kinetics.

This interpretation is supported by the study of Voronkov and Falster,[25] who demonstrated that hydrogen in c-Si participates in a dynamic network of metastable monomers and dimers with distinct diffusivities and dissociation pathways. While stable trapping is absent, the dominant charge state of hydrogen, which varies with the doping condition, governs which of these transient configurations and reaction pathways are accessible.[23] As a result, the effective diffusivity becomes a weighted average of the hydrogen migration kinetics. Additionally, brief electrostatic interactions with charged dopants may further perturb the local migration paths of these hydrogen species, contributing to the overall modification of the effective hydrogen diffusivity.

Finally, we consider the potential role of interface effects. The spread in the reported hydrogen diffusivity values may also be influenced by variations in the interface preparation across different studies. Fermi-level pinning at the Si semiconductor boundaries can create band bending and a space-charge region, which introduces a drift component to the transport of charged hydrogen species.[48] This mechanism is most pronounced for interfaces where band bending is deliberately induced, such as by ion bombardment. In the present work, the interfaces were formed by thin Si film deposition without such treatments. As a result, while interface effects may contribute to the cross-laboratory discrepancy in the literature, the systematic variation in the effective hydrogen diffusivity captured in this study is ascribed primarily to differences in the c-Si bulk transport.

This measurement method used in this work for effective hydrogen diffusivity involves several inherent limitations due to thermal constraints imposed by the material properties of the test structures. First, de-hydrogenation becomes dominant at annealing temperatures above 500 °C, preventing the deposited Si films from effectively capturing hydrogen. Second, it was observed that hydrogenated Al_2O_3 layers require annealing temperatures above 300 °C to release hydrogen effectively. Third, prolonged annealing durations can cause hydrogen to effuse into the ambient before sufficient accumulation occurs in the Si films to produce a measurable hydrogenation effect. This was observed when measuring hydrogen diffusivity in heavily doped n- and p-type samples at 350 °C, where the extended annealing durations of 4–5 h led to a significant decrease in hydrogen concentrations before reaching the steady state. Under such conditions, the hydrogen profiles become difficult to interpret, and hence, the diffusion modeling becomes unreliable. In Fig. 7, the extracted hydrogen diffusivities in p-type Si in this work are greater than other studies showing diffusivities in p-type Si. A possible reason is that PAALD was carried out for 25 min at 200 °C where some hydrogen may have diffused into the Si bulk, causing an overestimation of hydrogen diffusivity. For thin c-Si wafer thicknesses of 75 μm used for p-type Si, such overestimation is likely more significant compared to thicker wafers of 150 and 350 μm. Nevertheless, this work reveals that hydrogen diffusivity in p-type Si is significantly reduced between 350 and 450 °C, as compared to the undoped and moderately doped n-type Si, which agrees reasonably with other published results.

VI. CONCLUSION

This work demonstrates an effective hydrogen diffusivity measurement method in c-Si using steady-state spectral PL and kinetic modeling. Sub-bandgap PL data were empirically correlated to relative hydrogen concentrations through ToF-SIMS. The method was first verified through measuring samples of different wafer thicknesses, which produced the same extracted hydrogen diffusivity values, as expected, confirming the approach. Effective diffusivity values measured in moderately doped n-type and undoped Si were found to agree well with Herring *et al.* The heavily doped n-type Si and all of the p-type Si wafers, however, displayed reduced effective diffusivity values, consistent with some literature that reported decreased hydrogen diffusivity values in c-Si with high defect densities, in heavily doped n-type or in p-type Si wafers. The hydrogen charge states in Si with different doping and at different temperatures were simulated. The reduced effective hydrogen diffusivity in heavily doped n-type Si and in all p-type Si may not be attributed to the formation of stable dopant–hydrogen complexes, as they dissociate rapidly at the high temperatures used in this work. Instead, the measured doping dependence is more plausibly explained by the influence of hydrogen charge states and their associated transient migration pathways. The dominant charge state, H^- in heavily doped n-type material and H^+ in p-type material, determines which metastable hydrogen configurations and reaction channels are accessible during diffusion. The cumulative effect of these distinct diffusion mechanisms can modify the effective hydrogen migration kinetics.

SUPPLEMENTARY MATERIAL

A detailed description of the mathematical model and parameters used for the diffusion kinetics analysis is provided in the supplementary material.

ACKNOWLEDGMENTS

This work was supported by the Australian Centre for Advanced Photovoltaics (ACAP). The authors thank Dr. Bill Bin Gong and Dr. Songyan Yin at the surface analysis laboratory, SSEAU, MWAC, UNSW, for performing ToF-SIMS measurements. The authors also thank Professor Gergely Zimanyi at UC Davis for helpful discussions about the possible impact of hydrogen charge states on diffusivity.

AUTHOR DECLARATIONS

Conflict of Interest

The authors have no conflicts to disclose.

Author Contributions

Zhuofeng Li: Conceptualization (equal); Data curation (equal); Formal analysis (equal); Methodology (equal); Software (equal); Validation (equal); Visualization (equal); Writing – original draft (equal); Writing – review & editing (equal). **Zhongshu Yang:** Methodology (equal); Software (equal); Writing – review & editing (equal). **Jiali Wang:** Data curation (equal); Validation (equal); Writing – review & editing (equal). **AnYao Liu:** Methodology (equal); Software (equal); Supervision (equal); Writing – review & editing (equal). **Areebah Murad:** Data curation (supporting). **Chang Sun:** Resources (equal). **Wei Han:** Resources (equal).

Yichun Wang: Resources (equal). **Hieu Nguyen:** Conceptualization (equal); Supervision (equal); Writing – review & editing (equal). **Daniel Macdonald:** Conceptualization (equal); Funding acquisition (equal); Project administration (equal); Supervision (equal); Writing – review & editing (equal).

DATA AVAILABILITY

The data that support the findings of this study are available from the corresponding authors upon reasonable request.

REFERENCES

[1]A. G. Aberle, "Overview on SiN surface passivation of crystalline silicon solar cells," Sol. Energy Mater. Sol. Cells **65**(1–4), 239–248 (2001).
[2]H. Mäckel and R. Lüdemann, "Detailed study of the composition of hydrogenated SiNx layers for high-quality silicon surface passivation," J. Appl. Phys. **92**(5), 2602–2609 (2002).
[3]F. Duerinckx and J. Szlufcik, "Defect passivation of industrial multicrystalline solar cells based on PECVD silicon nitride," Sol. Energy Mater. Sol. Cells **72**(1–4), 231–246 (2002).
[4]B. J. Hallam *et al.*, "Hydrogen passivation of B–O defects in Czochralski silicon," Energy Procedia **38**, 561–570 (2013).
[5]B. J. Hallam *et al.*, "Advanced hydrogenation of dislocation clusters and boron-oxygen defects in silicon solar cells," Energy Procedia **77**, 799–809 (2015).
[6]B. Hallam, C. Chan, M. Abbott, and S. Wenham, "Hydrogen passivation of defect-rich n-type Czochralski silicon and oxygen precipitates," Sol. Energy Mater. Sol. Cells **141**, 125–131 (2015).
[7]J.-F. Lelièvre, E. Fourmond, A. Kaminski, O. Palais, D. Ballutaud, and M. Lemiti, "Study of the composition of hydrogenated silicon nitride SiNx: H for efficient surface and bulk passivation of silicon," Sol. Energy Mater. Sol. Cells **93**(8), 1281–1289 (2009).
[8]G. Krugel, W. Wolke, J. Geilker, S. Rein, and R. Preu, "Impact of hydrogen concentration on the regeneration of light induced degradation," Energy Procedia **8**, 47–51 (2011).
[9]J. Schmidt, A. Merkle, R. Brendel, B. Hoex, M. C. M. V. de Sanden, and W. M. M. Kessels, "Surface passivation of high-efficiency silicon solar cells by atomic-layer-deposited Al_2O_3," Prog. Photovoltaics Res. Appl. **16**(6), 461–466 (2008).
[10]B. Hoex, J. Schmidt, P. Pohl, M. C. M. V. de Sanden, and W. M. M. Kessels, "Silicon surface passivation by atomic layer deposited Al_2O_3," J. Appl. Phys. **104**(4), 044903 (2008).
[11]C. Herring, N. M. Johnson, and C. G. Van de Walle, "Energy levels of isolated interstitial hydrogen in silicon," Phys. Rev. B **64**(12), 1252091–12520927 (2001).
[12]A. Van Wieringen and N. Warmoltz, "On the permeation of hydrogen and helium in single crystal silicon and germanium at elevated temperatures," Physica **22**(6–12), 849–865 (1956).
[13]T. Ichimiya and A. Furuichi, *On the Solubility and Diffusion Coefficient of Tritium in Single Crystals of Silicon* (Pergamon Press, 1968).
[14]A. Mogro-Campero, R. P. Love, and R. Schubert, "Drastic changes in the electrical resistance of gold-doped silicon produced by a hydrogen plasma," J. Electrochem. Soc. **132**(8), 2006 (1985).
[15]M. Capizzi and A. Mittiga, "Hydrogen in Si: Diffusion and shallow impurity deactivation," Physica B+C **146**, 19–29 (1987).
[16]C. H. Seager, R. A. Anderson, and D. K. Brice, "*In situ* measurements of hydrogen motion and bonding in silicon," J. Appl. Phys. **68**(7), 3268–3284 (1990).
[17]C. P. Herrero, M. Stutzmann, A. Breitschwerdt, and P. V. Santos, "Trap-limited hydrogen diffusion in doped silicon," Phys. Rev. B **41**(2), 1054 (1990).
[18]Y. V. Gorelkinskii and N. N. Nevinnyi, "Electron paramagnetic resonance of hydrogen in silicon," Physica B **170**(1–4), 155–167 (1991).
[19]T. Zundel and J. Weber, "Trap-limited hydrogen diffusion in boron-doped silicon," Phys. Rev. B **46**(4), 2071 (1992).
[20]R. Rizk, P. De Mierry, D. Ballutaud, M. Aucouturier, and D. Mathiot, "Hydrogen diffusion and passivation processes in p-and n-type crystalline silicon," Phys. Rev. B **44**(12), 6141 (1991).
[21]K. J. Chang and D. J. Chadi, "Hydrogen bonding and diffusion in crystalline silicon," Phys. Rev. B **40**(17), 11644 (1989).
[22]L. Bilteanu, M. Posselt, and J.-P. Crocombette, "Hydrogen diffusion in silicon—An *ab initio* study of hydrogen kinetic properties in silicon," arXiv:1111.6455 (2011).
[23]S. K. Estreicher, A. Docaj, M. B. Bebek, D. J. Backlund, and M. Stavola, "Hydrogen in C-rich Si and the diffusion of vacancy–H complexes," Phys. Status Solidi A **209**(10), 1872–1879 (2012).
[24]S. J. Pearton, J. W. Corbett, and T. S. Shi, "Hydrogen in crystalline semiconductors," Appl. Phys. A **43**, 153–195 (1987).
[25]V. V. Voronkov and R. Falster, "Formation, dissociation, and diffusion of various hydrogen dimers in silicon," Phys. Status Solidi B **254**(6), 1600779 (2017).
[26]P. Hamer, B. Hallam, R. S. Bonilla, P. P. Altermatt, P. Wilshaw, and S. Wenham, "Modelling of hydrogen transport in silicon solar cell structures under equilibrium conditions," J. Appl. Phys. **123**(4), 043108 (2018).
[27]P. Vieira Rodrigues *et al.*, "Doping dependence of boron–hydrogen dynamics in crystalline silicon," J. Appl. Phys. **136**(8), 085703 (2024).
[28]J. Schön, P. Hamer, B. Hammann, C. Zechner, W. Kwapil, and M. C. Schubert, "Hydrogen in silicon solar cells: The role of diffusion," Sol. RRL **9**(1), 2400668 (2025).
[29]M. Taguchi *et al.*, "24.7% record efficiency HIT solar cell on thin silicon wafer," IEEE J. Photovoltaics **4**(1), 96–99 (2014).
[30]X. Ru *et al.*, "25.11% efficiency silicon heterojunction solar cell with low deposition rate intrinsic amorphous silicon buffer layers," Sol. Energy Mater. Sol. Cells **215**, 110643 (2020).
[31]D. E. Carlson and C. W. Magee, "A SIMS analysis of deuterium diffusion in hydrogenated amorphous silicon," Appl. Phys. Lett. **33**(1), 81–83 (1978).
[32]M. Sheoran *et al.*, "Hydrogen diffusion in silicon from plasma-enhanced chemical vapor deposited silicon nitride film at high temperature," Appl. Phys. Lett. **92**(17), 172107 (2008).
[33]Z. Zhu, V. Shutthanandan, and M. Engelhard, "An investigation of hydrogen depth profiling using ToF-SIMS," Surf. Interface Anal. **44**(2), 232–237 (2012).
[34]B. Paudel *et al.*, "ToF-SIMS in material research: A view from nanoscale hydrogen detection," Mater. Today **75**, 149–165(2024).
[35]D. Engemann and R. Fischer, "Photoluminescence in amorphous silicon," Phys. Status Solidi B **79**(1), 195–202 (1977).
[36]H. T. Nguyen *et al.*, "Characterizing amorphous silicon, silicon nitride, and diffused layers in crystalline silicon solar cells using micro-photoluminescence spectroscopy," Sol. Energy Mater. Sol. Cells **145**, 403–411 (2016).
[37]H. T. Nguyen *et al.*, "Sub-bandgap luminescence from doped polycrystalline and amorphous silicon films and its application to understanding passivating-contact solar cells," ACS Appl. Energy Mater. **1**(11), 6619–6625 (2018).
[38]H. Hieslmair, S. Balasubramanian, A. A. Istratov, and E. R. Weber, "Gettering simulator: Physical basis and algorithm," Semicond. Sci. Technol. **16**(7), 567–574 (2001).
[39]A. Liu *et al.*, "Understanding the impurity gettering effect of polysilicon/oxide passivating contact structures through experiment and simulation," Sol. Energy Mater. Sol. Cells **230**, 111254 (2021).
[40]C. Sun, F. E. Rougieux, and D. Macdonald, "A unified approach to modelling the charge state of monatomic hydrogen and other defects in crystalline silicon," J. Appl. Phys. **117**(4), 045702 (2015).
[41]M. J. Kerr and A. Cuevas, "Recombination at the interface between silicon and stoichiometric plasma silicon nitride," Semicond. Sci. Technol. **17**(2), 166 (2002).
[42]T. N. Truong *et al.*, "Hydrogenation of phosphorus-doped polycrystalline silicon films for passivating contact solar cells," ACS Appl. Mater. Interfaces **11**(5), 5554–5560 (2019).
[43]N. Budini, P. A. Rinaldi, J. A. Schmidt, R. D. Arce, and R. H. Buitrago, "Influence of microstructure and hydrogen concentration on amorphous silicon crystallization," Thin Solid Films **518**(18), 5349–5354 (2010).

[44]J. N. Lee, B. J. Lee, D. G. M. Dae Gyu Moon, and B. T. A. Byung Tae Ahn, "Effect of deposition temperature on the crystallization mechanism of amorphous silicon films on glass," Jpn. J. Appl. Phys. **36**(11R), 6862 (1997).
[45]T. N. Truong *et al.*, "Deposition pressure dependent structural and opto-electronic properties of ex-situ boron-doped poly-Si/SiOx passivating contacts based on sputtered silicon," Sol. Energy Mater. Sol. Cells **215**, 110602 (2020).
[46]J. Crank and P. Nicolson, "A practical method for numerical evaluation of solutions of partial differential equations of the heat-conduction type," Math. Proc. Cambridge Philos. Soc. **43**, 50–67 (1947).
[47]B. J. Hallam *et al.*, "Advanced bulk defect passivation for silicon solar cells," IEEE J. Photovoltaics **4**(1), 88–95 (2013).
[48]K. Dev, M. Y. L. Jung, R. Gunawan, R. D. Braatz, and E. G. Seebauer, "Mechanism for coupling between properties of interfaces and bulk semiconductors," Phys. Rev. B **68**(19), 195311 (2003).